atmosphere

MDPI

Article

Spatial Particulate Fields during High Winds in the Imperial Valley, California

Frank R. Freedman [1,*], Paul English [2], Jeff Wagner [3], Yang Liu [4], Akula Venkatram [5], Daniel Q. Tong [6], Mohammad Z. Al-Hamdan [7], Meytar Sorek-Hamer [8], Robert Chatfield [9], Ana Rivera [10] and Patrick L. Kinney [11]

[1] Department of Meteorology and Climate Science, San Jose State University, San Jose, CA 95192, USA
[2] Environmental Health Investigations Branch, California Department of Public Health, Richmond, CA 94804, USA; Paul.English@cdph.ca.gov
[3] Environmental Health Laboratory, California Department of Public Health, Richmond, CA 94804, USA; jeff.wagner@cdph.ca.gov
[4] Department of Environmental Health, Rollins School of Public Health, Emory University, Atlanta, GA 30322, USA; yang.liu@emory.edu
[5] Department of Mechanical Engineering, University of California at Riverside, Riverside, CA 92521, USA; venky@engr.ucr.edu
[6] Center for Spatial Information Science and Systems, George Mason University, Fairfax, VA 22030, USA; qtong@gmu.edu
[7] Universities Space Research Association, NASA Marshall Space Flight Center, Huntsville, AL 35805, USA; mohammad.alhamdan@nasa.gov
[8] Universities Space Research Association, NASA Ames Research Center, Mountain View, CA 94043, USA; meytar.sorekhamer@nasa.gov
[9] NASA Ames Research Center, Mountain View, CA 94043, USA; robert.b.chatfield@nasa.gov
[10] Department of Geography, Environment and Spatial Sciences, Michigan State University, East Lansing, MI 48824, USA; rivera59@msu.edu
[11] School of Public Health, Boston University, Boston, MA 02215, USA; pkinney@bu.edu
* Correspondence:frank.freedman@sjsu.edu

Received: 14 November 2019; Accepted: 2 January 2020; Published: 10 January 2020

Abstract: We examined windblown dust within the Imperial Valley (CA) during strong springtime west-southwesterly (WSW) wind events. Analysis of routine agency meteorological and ambient particulate matter (PM) measurements identified 165 high WSW wind events between March and June 2013 to 2019. The PM concentrations over these days are higher at northern valley monitoring sites, with daily PM mass concentration of particles less than 10 micrometers aerodynamic diameter (PM10) at these sites commonly greater than 100 μg/m^3 and reaching around 400 μg/m^3, and daily PM mass concentration of particles less than 2.5 micrometers aerodynamic diameter (PM2.5) commonly greater than 20 μg/m^3 and reaching around 60 μg/m^3. A detailed analysis utilizing 1 km resolution multi-angle implementation of atmospheric correction (MAIAC) aerosol optical depth (AOD), Identifying Violations Affecting Neighborhoods (IVAN) low-cost PM2.5 measurements and 500 m resolution sediment supply fields alongside routine ground PM observations identified an area of high AOD/PM during WSW events spanning the northwestern valley encompassing the Brawley/Westmorland through the Niland area. This area shows up most clearly once the average PM10 at northern valley routine sites during WSW events exceeds 100 μg/m^3. The area is consistent with high soil sediment supply in the northwestern valley and upwind desert, suggesting local sources are primarily responsible. On the basis of this study, MAIAC AOD appears able to identify localized high PM areas during windblown dust events provided the PM levels are high enough. The use of the IVAN data in this study illustrates how a citizen science effort to collect more spatially refined air quality concentration data can help pinpoint episodic pollution patterns and possible sources important for PM exposure and adverse health effects.

Keywords: windblown dust; particulate matter; PM10; PM2.5; Imperial Valley; MAIAC; IVAN; sediment supply

1. Introduction

The Imperial Valley, which is an agriculturally dominated area located in Southeastern California adjacent to the US-Mexico border, has among the highest particulate matter (PM) air pollution concentrations in the United States. The area has historically been nonattainment with respect to both PM10 (PM mass concentration of particles less than 10 micrometers aerodynamic diameter) and PM2.5 (PM mass concentration of particles less than 2.5 micrometers aerodynamic diameter) ambient air standards [1,2]. Imperial County also has the highest rates of asthma emergency room visits and hospitalization among school-age children of all counties in California [3]. The PM2.5 fraction yields the strongest correlations with respiratory and cardiovascular health effects due to the ability of these fine particles to penetrate deep into the lungs [4]. Larger PM10 particles deposit in the nose and upper airways and are associated with increased inflammation, asthma, and respiratory effects [5,6]. Windblown dust, which is a particularly important component of coarse PM10, has been associated with a variety of adverse health effects, including cardiovascular mortality [7], heart attacks [8], and *Coccidioidomycosis*, commonly known as Valley Fever, an infection caused by inhalation of a soil-dwelling fungus. Valley Fever has increased in incidence by 800% from 1998 to 2011 across the United States, with much of this increase in the southwestern U.S., where windblown dust is common [9,10].

Windblown dust is a major cause of high PM in the Imperial Valley. Strong, gusty winds in the area are common throughout the year associated with passing storm systems, persistent low-pressure systems, and summer monsoonal flows. Chow et al. [11] analyzed PM10 measurements in 1992 and 1993 over the Calexico-Mexicali area, finding that fugitive dust comprised roughly 70% of total PM10 at both sites over the data period. Wagner and Casuccio [12] used electron microscopy to analyze regulatory PM10 and PM2.5 filter samples from Imperial Valley to determine composition and source contributions. They found that the filters were dominated by large crustal particles up to 30 μm in diameter that matched local soils, and that windblown dust was a major source on high PM days. Windblown dust in the area has also been extensively investigated with respect to the increasing importance of dust emissions from exposed beds of the Salton Sea, which bounds the valley to the north [13–18]. Windblown dust events also lead to PM10 regulatory exceedances in the air basin [19].

The most common type of windblown dust event in the valley is due to west-southwesterly (WSW) winds associated with low pressure systems off the Pacific coast. These situations are most common during spring and are responsible for most of the PM10 regulatory exceedances in the area [19]. Here, we will refer to these as WSW windblown dust events. While there is a general understanding that WSW events cause high PM in the valley, a detailed analysis focusing on their underlying spatial PM patterns across the valley utilizing newly available high-resolution datasets is now possible. Knowledge of areas of the valley most prone to high PM during WSW events would be useful to reduce human exposure during these conditions.

In this paper, we present a data analysis of WSW windblown dust events that occurred in the Imperial Valley over recent years with the aim to better understanding their fine-scale spatial patterns. The study is divided into two parts. First, we present the basic meteorology and ambient PM10 and PM2.5 conditions of WSW events based on analysis of routine government agency meteorological and ambient air PM10 and PM2.5 measurements in order to provide a basic understanding and context. Then, we present a detailed analysis of spatial PM patterns utilizing, alongside routine observations, the following three recent high-resolution datasets: PM2.5 measurements from Identifying Violations Affecting Neighborhoods (IVAN) "low-cost" network [20–22], remotely sensed aerosol optical depth (AOD) from the NASA 1 km multi-angle implementation of atmospheric correction (MAIAC) product [23], and 500 m soil sediment fields from Parajuli and Zender [24]. In addition to the main goal of providing a more detailed depiction of spatial PM

patterns associated with these events, the experience presented in this paper utilizing these high-resolution datasets to examine local hotspots of windblown PM can be beneficial for similar analysis in other locations.

Section 2 presents details of the data used and methodology. Then, Section 3 presents the routine data analysis of WSW windblown dust events utilizing only standard government agency observations over the years 2013 to 2019, the detailed analysis of spatial PM patterns incorporating alongside routine observations IVAN PM2.5, MAIAC AOD, and sediment supply data over the years 2014 to 2017, and a discussion of possible implied source areas of the windblown dust during events. Finally, Section 4 summarizes our work.

2. Data and Methods

Figure 1 is a map of the study area, showing the locations of routine state agency PM10 and PM2.5 monitors, IVAN PM2.5 ambient air monitors, and the Imperial County Airport National Weather Service meteorological station (KIPL).

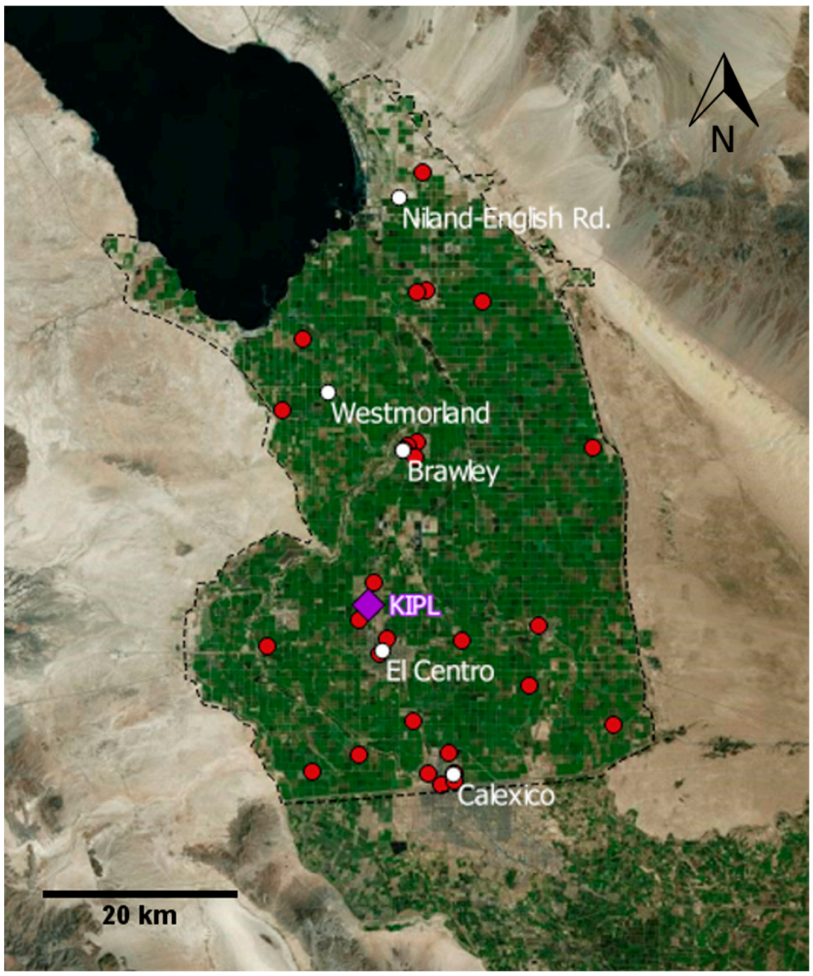

Figure 1. Map of the study area: Particulate matter (PM) mass concentration of particles less than 10 micrometers aerodynamic diameter (PM10) and PM mass concentration of particles less than 2.5 micrometers aerodynamic diameter (PM2.5) ambient air concentration measurement site locations (**white dots**), Identifying Violations Affecting Neighborhoods (IVAN) PM2.5 data site locations (**red dots**), and the Imperial County Municipal Airport National Weather Service meteorological site location (KIPL) (**purple diamond**). The black dashed line surrounding the Imperial Valley is used to mask the MAIAC AOD fields to retain pixels only within the valley.

2.1. Routine Data

Routine state agency ambient air PM data were downloaded from the California Air Resources Board Air Quality and Meteorological Information System [25]. Wind data at KIPL were downloaded from Mesowest [26]. State agency PM10 and PM2.5 measurements are available at the following five sites (see Figure 1): Niland-English Road, Westmorland, Brawley, El Centro, and Calexico. Table 1 provides details, indicating time periods of availability for each site over the study period. The PM10 measurements were from continuous hourly beta-attenuation monitors (BAMS) at each of the five sites. The PM2.5 measurements were from both daily-averaged gravimetric monitors at three of the five sites (Calexico, El Centro, and Brawley), and from hourly continuous BAMS monitors at two of the five sites (Calexico and Niland-English Road). The time periods of availability depend on the site. The data analysis period starts in 2013 to correspond to the year that PM10 BAMS sites began operating.

Table 1. Ground-level ambient-air PM data utilized.

Data	Sites	Time Period
Routine PM10–hourly (BAMS) [1]	Niland-English Ed.	2013–2019
	Westmorland	2016–2019
	Brawley	2013–2019
	El Centro	2016–2019
	Calexico	2016–2019
Routine PM2.5–daily (Gravimetric) [1]	Brawley	2013–2019
	El Centro	2013–2019
	Calexico	2013–2019
Routine PM2.5–hourly (BAMS) [1]	Niland-English Rd.	2016–2017
	Calexico	2014–2017
IVAN PM2.5–hourly (Modified DYLOS 1700 particle counts [2])	See Figure 1 for locations	2016 (14 sites)
		2017 (29 sites)

[1] Routine PM10 and PM2.5 data were obtained from https://www.arb.ca.gov/aqmis2/aqmis2.php.; [2] See Carvlin et al. [21] for method of translating particle counts to PM2.5..

2.2. High Resolution Data

2.2.1. IVAN

The Identifying Violations Affecting Neighborhoods (IVAN) low-cost PM monitoring network (https://ivan-imperial.org/air) was developed as a NIH-funded collaboration of community, academic, nongovernmental, and governmental partners designed to augment state PM measurements in the Imperial Valley [20]. The PM is measured in real time at 40 sites over Imperial County. The monitors are modified Dylos 1700 optical PM sensors, and provide five minute particle counts at four size bins, i.e., >0.5, >1, >2.5, and >10 μm. The data are hourly-averaged, and hourly PM2.5 mass concentrations are determined by use of an empirical relationship derived from co-located IVAN and PM2.5 measurements at the Calexico state-agency site [21]. The IVAN monitors first came online in 2016, with the full suite operating by 2017. IVAN data were provided to us through a formal public request as part of a collaboration with IVAN principals formed from NASA Health and Air Quality Applied Science Team "Tiger Team" work (https://haqast.org/, http://sites.bu.edu/haqast-highrestt/). We utilized IVAN measurements at sites located within the U.S. portion of the valley, excluding sites outside the valley and immediately adjacent to the Salton Sea, where high quality MAIAC AOD retrievals are less consistent. Therefore, the number of utilized IVAN sites (29) was less than the network total (40).

2.2.2. MAIAC

The NASA multi-angle implementation for atmospheric correction (MAIAC) product [24] provides remotely sensed measurements of several surface and aerosol related variables derived from Level 1B five minute MODIS top-of-atmosphere reflectance retrievals collected by Terra and Aqua polar orbiting satellites. From this suite, we utilized aerosol optical depth (AOD) at 550 nm, a measure of total column aerosol mass abundance for cloud-free conditions inferred from measured MODIS retrievals of passive solar reflectance at this wavelength. The MAIAC AOD fields are globally available at 1 km horizontal resolution daily for both Terra (between 1000 and 1200 LST depending on day) and Aqua (between 1200 and 1400 LST depending on day) retrievals. We utilized data from Aqua since these overpasses occur in the afternoon, at the beginning of the typical afternoonthrough evening concentration buildup period during WSW windblown dust events. The MAIAC fields can be obtained at the NASA LAADS-DAAC server [27].

2.2.3. Sediment Supply

Surface sediment supply is a unitless indicator ranging from 0 to 1, linearly related to windblown dust emission flux. Sediment supply fields across and around the Imperial Valley were taken from the global 500 m resolution dataset of Parajuli and Zender [24]. This dataset was developed by combining HydroBASINS upstream catchment and MODIS blue-band surface reflectance.

2.3. Method

The following two analyses were performed: a routine analysis using state agency measurements (hereafter called "routine data") to provide a background understanding of WSW windblown dust events, and a detailed analysis focusing on fine-scale spatial PM patterns utilizing, in addition to routine data, IVAN, MAIAC, and sediment supply measurements.

For the routine analysis, WSW events were selected as days within March to June from 2013 to 2019 when the daily average wind speed was greater than 10 mph and the wind direction for at least ten hours was within 230 to 280 degrees, using hourly winds at KIPL. From inspection of plots of the monitoring data, hourly winds greater than 10 mph and within 230 to 280 degrees at KIPL correspond to the hours of highest PM10 at routine monitoring sites over the area. A daily average wind speed of 10 mph for ten or more hours per day within 230 to 280 degrees was then selected as a relatively simple criteria that was successful in selecting high PM10 events due to WSW winds for subsequent analysis. This selection procedure yielded 165 days from 2013 to 2019, when two of the five continuous BAMS PM10 sites were operating (Brawley and Niland), and 104 days from 2016 to 2019, when all five BAMS PM_{10} sites were operating. Within this larger set was a subset when gravimetric PM2.5 measurements were also available from one-in-three monitoring at Brawley (57 days between 2013 and 2019), Calexico (55 days between 2013 and 2019), and El Centro (55 days between 2013 and 2019).

For the detailed analysis, we analyzed a subset of events from 2014 to 2017. Here, cases were selected as occurring from March through June when the KIPL wind speed averaged over 1200 to 1400 LST was above 10 mph and the wind direction scalar averaged over these hours was between 230 and 280 degrees. The 1200 to 1400 LST period was chosen to cover the Aqua satellite overpass time. . From this procedure, 82 days were identified. From this larger set, we produced a WSW set of 31 days when AOD spatial coverage was sufficiently complete across the valley for further analysis. Only cloud-free, highest quality flagged AOD pixels were used, and fields were masked to only include pixels within the valley to exclude those in surrounding bright desert areas where retrieval quality was less reliable. Plots of PM10 concentrations at Brawley and Niland BAMS sites (Figure A1) show that PM conditions for the chosen 31 days are reasonably representative of the larger 82 day set. The AOD and PM fields (routine and IVAN) of these 31 cases were then analyzed, focusing on spatial patterns. To guide interpretation, a control set of low-to-moderate southeasterly (SE) wind days, characteristic of lower, typical PM concentrations for spring, was constructed using the same method as days during March through June 2014 to 2017 and 1200 to 1400 LST when KIPL wind speed was 8 mph or less and between 100 and 150 degrees. This procedure produced a SE set of 47 days. Table 2 presents a summary of the WSW and SE sets for detailed analysis.

Table 2. Data summary and detailed analysis.

WSW						
Year	**Number of Days**	**WSPD (mph)**	**WDIR (deg)**	**PM_{10} ($\mu g/m^3$)**	**Number of AOD-PM2.5 Pairs (IVAN)**	**Number of AOD-PM10 Pairs (Routine)**
2014	11	18	234	130	-	19 over 2 sites
2015	2	21	265	230	-	2 over 1 site
2016	11	17	248	139	99 over 11 sites	46 over 5 sites
2017	7	18	259	85	149 over 29 sites	32 over 5 sites
Total/Avg	31	18	247	130	248 over 29 sites	99 over 5 sites
SE						
Year	**Number of Days**	**WSPD (mph)**	**WDIR (deg)**	**PM_{10} ($\mu g/m^3$)**	**Number of AOD-PM2.5 Pairs (IVAN)**	**Number of AOD-PM10 Pairs (Routine)**
2014	13	6	125	36	-	20 over 2 sites
2015	12	7	100	29	-	16 over 2 sites
2016	12	7	104	32	108 over 11 sites	55 over 5 sites
2017	10	8	106	30	240 over 29 sites	49 over 5 sites
Total/Avg	47	7	108	32	348 over 29 sites	140 over 5 sites

[1] WSPD, WDIR, and PM10 are averages over 1200 to 1400 LST. WSPD and WDIR are from KIPL measurements. PM10 are averages of Brawley and Niland-English Rd. routine site measurements.

3. Results and Discussion

3.1. Routine Analysis

The common occurrence of strong WSW winds in the valley is shown in Figure 2, which presents histograms of the hours of high wind speed (greater than 10 mph) at KIPL organized by wind direction and month. Strong winds from the west-southwesterly sector (230° to 300°) occur over all months but are most common during the spring. The other main period of high wind speed is in the summer from the southeasterly sector (100° to 150°), associated with the summer monsoonal flow from the Gulf of California.

The large-scale meteorological forcing of WSW wind events is broadly associated with cyclonic winds around large-scale low-pressure systems with trough axis just offshore or along the California coast. Examples are seen in Figure 3, which show the 700 mb geopotential height fields from the North American Regional Reanalysis [28] for four events. The 20140521, 20150522, and 20160526 charts in this figure illustrate these low-pressure systems. These can be associated with relatively fast synoptic frontal passages, more persistent, slower moving large-scale troughs, or hybrid combinations of these two. The chart for 20170506 illustrates a different situation, with the low-pressure system weaker, more diffuse, and centered further east in the U.S. upper Midwest. Anti-cyclonic flow around a strong, high amplitude ridge offshore of the Pacific Northwest is more likely to be the driving forcing in this case. Overall, strong surface pressure gradients associated with large-scale pressure systems in the western U.S., most often low pressure centered in California, drive episodic strong WSW wind events in the Imperial Valley.

Plots of daily PM10 versus wind speed at each BAMS site over the days identified for routine analysis (Section 2.3) are shown in Figure 4. Concentrations are overall higher at the northern valley sites (Brawley, Westmorland, and Niland), with the highest values reaching around 400 $\mu g/m^3$ at these sites as compared with 200 $\mu g/m^3$ at the southern sites (El Centro and Calexico). The daily PM10 is positively correlated with wind speed at all sites, characteristic of windblown dust; however, there is significant scatter, ($r^2 < 0.3$ at all sites). This large variability could indicate variations of dust emissions, which can span two to three orders of magnitudes at fixed wind speed [13]. Plots of PM10 versus wind speed using the underlying hourly measurements show similar behavior and variability (not shown for brevity).

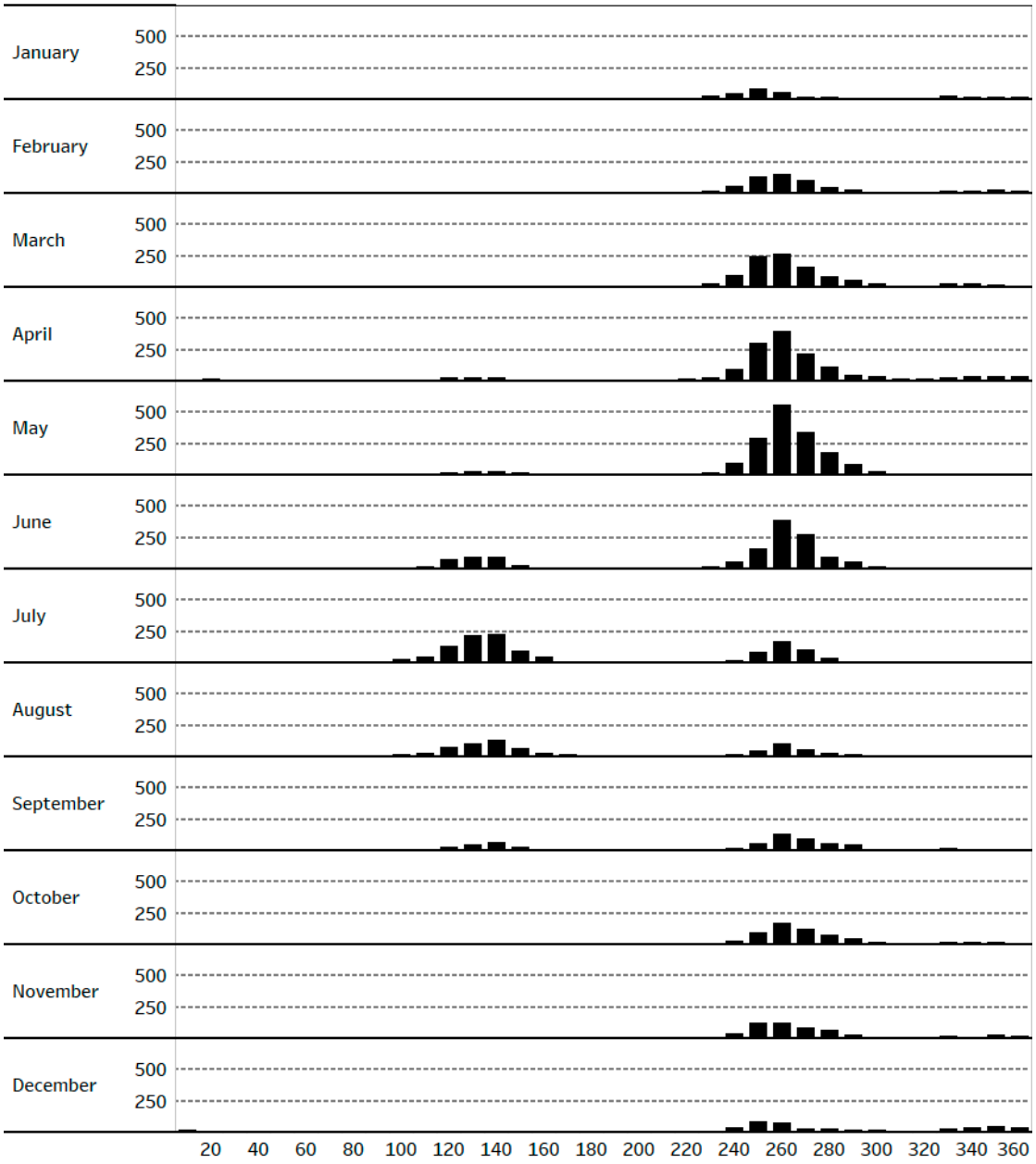

Figure 2. Monthly wind direction histograms of hours when wind speed is greater than 10 mph, as measured at the Imperial County Municipal Airport (KIPL). Data period 2010 to 2017.

Plots of daily PM2.5 versus wind speed at each gravimetric site are shown in Figure 5. Consistent with PM10, concentrations are higher at Brawley than El Centro and Calexico. Concentrations often exceed 20 μg/m^3 at Brawley with the highest value reaching around 60 μg/m^3 but rarely exceeding 20 μg/m^3 at El Centro and Calexico. The daily PM2.5 is positively correlated with wind speed at all sites, however with lower r^2 as compared with PM10. This is consistent with the weaker association of PM2.5 with windblown dust as compared with PM10.

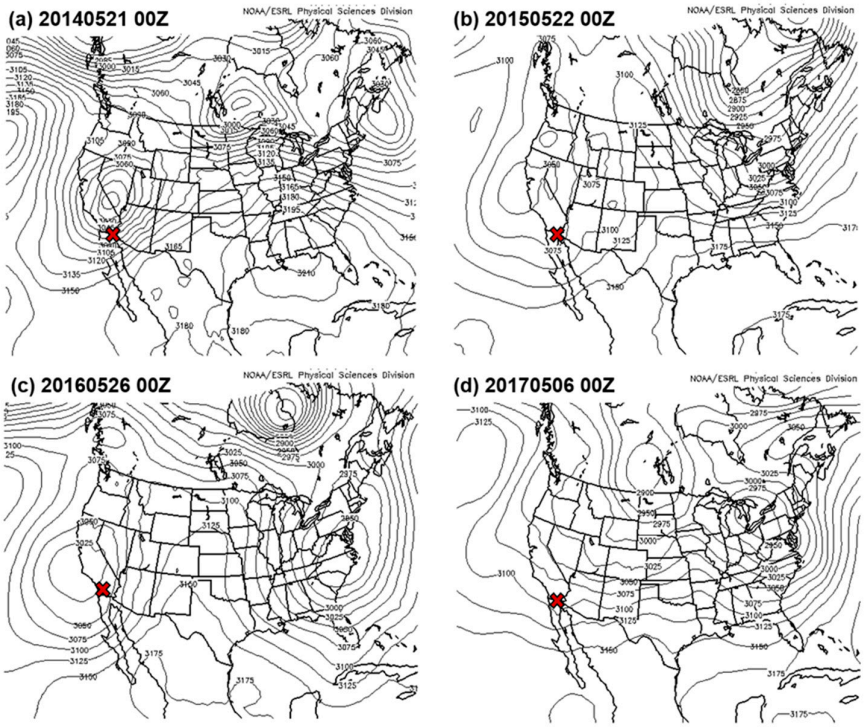

Figure 3. The 700 mb geopotential height fields (meters) from the North American Regional Reanalysis [28] for four west-southwesterly (WSW) high wind events affecting the Imperial Valley. The red X on each panel is the approximate location of valley. Plots were created from the NARR plotting website operated by NOAA/OAR/ESRL PSD, Boulder, Colorado, USA (https://www.esrl.noaa.gov/psd/data/gridded/data.narr.html).

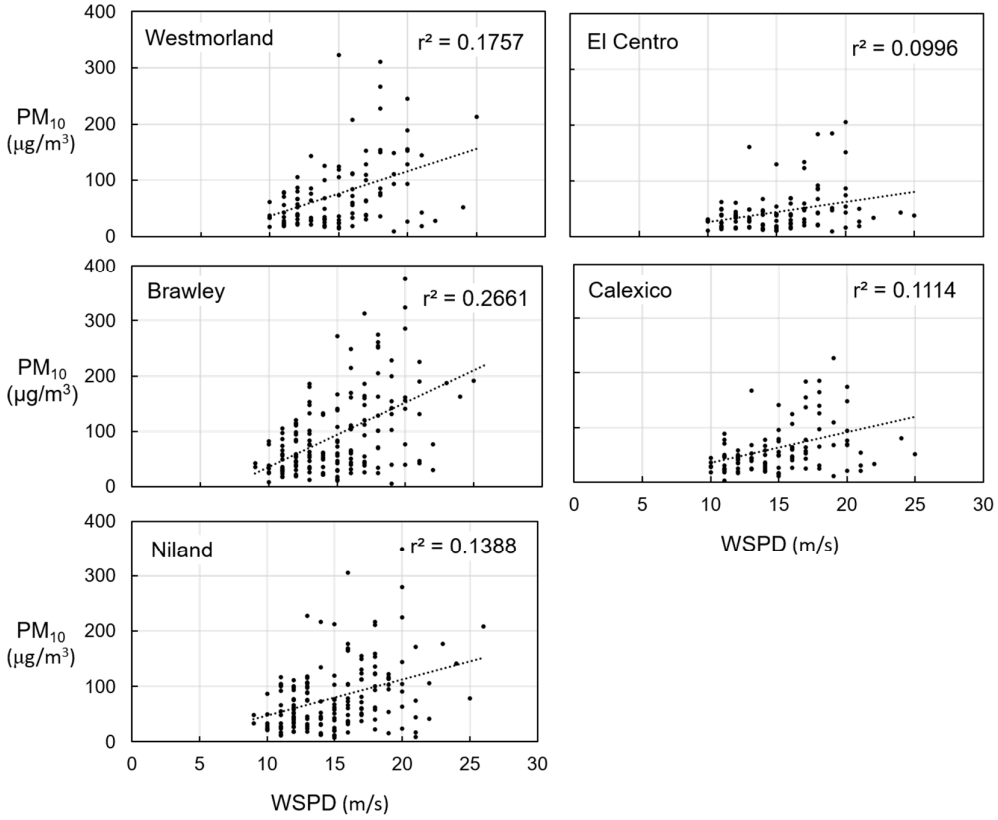

Figure 4. Daily averaged beta-attenuation monitors (BAMS) PM10 concentrations versus daily-averaged wind speed at KIPL for the selected springtime WSW wind events in the Imperial Valley. The coefficient of determination (r^2) of the plotted best-fit regression line is indicated on each panel. Data comprise 165 days between 2013 and 2019 for Brawley and Niland, and 104 days between 2016 and 2019 for Calexico, El Centro, and Westmorland. Criteria of event selection is given in Section 2.3.

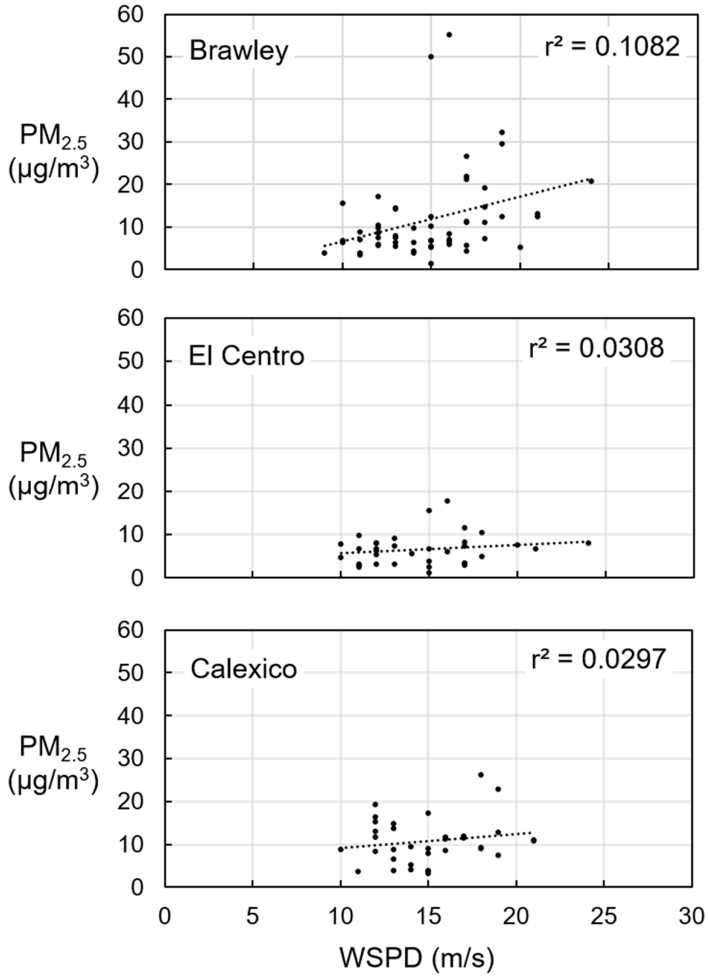

Figure 5. Daily averaged gravimetric PM2.5 concentrations versus daily-averaged wind speed at KIPL for selected springtime WSW wind events in the Imperial Valley. The coefficient of determination (r^2) of the plotted best-fit regression line is indicated on each panel. Data comprise 57 daily events between 2013 and 2019 at Brawley, and 55 daily events between 2013 and 2019 for Calexico and El Centro. Criteria of event selection is given in Section 2.3.

3.2. Detailed Analysis: IVAN, MAIAC, Sediment Supply

This section presents an analysis of a subset of WSW events from 2014 to 2017 utilizing high-resolution datasets aimed at more precisely defining the spatial patterns of PM across the valley typical during WSW events. A set of 31 WSW and 47 SE control events are analyzed. See Section 2.2 and 2.3 for details on the datasets and methodology, respectively.

The average MAIAC AOD fields of the WSW and SE sets are shown in Figure 6. The AOD across the valley is higher in the WSW set, consistent with its higher PM associated with windblown dust (Table 2). The most distinguishing spatial feature is the swath of relatively high AOD (≈ 0.15 and higher) spanning the northwestern valley across the Brawley/Westmorland to Niland area, with lower AOD across the southern and southeastern valley through El Centro and Calexico. This is consistent with the higher PM10 and PM2.5 concentrations at the northern valley routine sites

(Section 3.1) but presents a clearer indication of the underlying spatial patterns. Excluding the band of high AOD along the western rim of the valley, there are two broad regions of AOD maxima, one around the Brawley/Westmorland area and another around and just south of Niland. Since the Brawley/Westmorland maximum does not appear in the SE control field, this appears to be a hotspot associated with windblown dust. The Niland area maximum, however, , is more uncertain since relatively high AOD in this area is also seen in the SE control field, although with a lower value. Several other patchy, localized areas of relatively high AOD common to both the WSW and SE sets can also be seen, for example, along a north-south strip running between Brawley to El Centro, the band of high AOD along the western rim of the valley, and patches of relatively high AOD around and just north of Calexico.

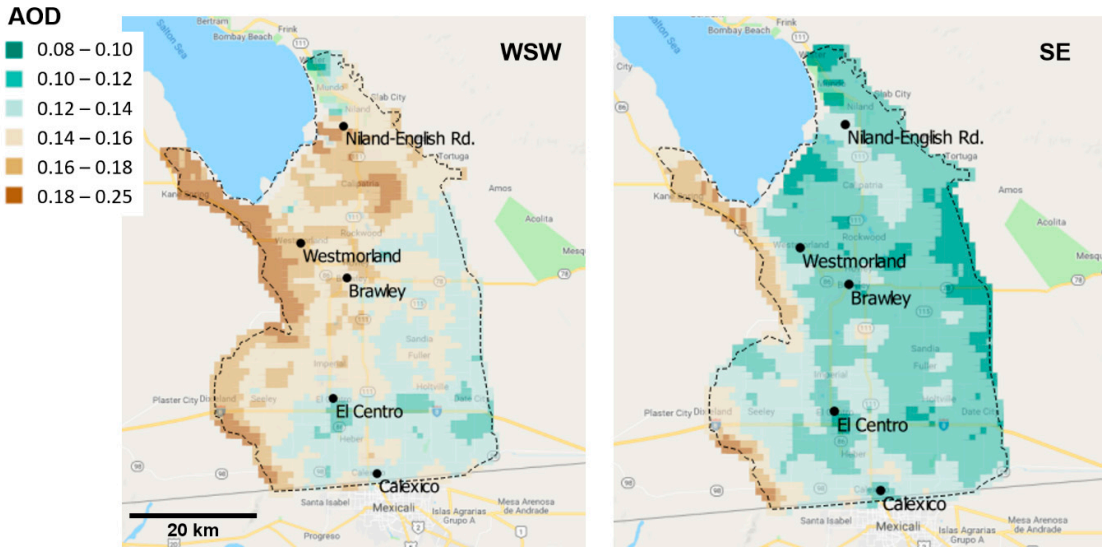

Figure 6. Average multi-angle implementation of atmospheric correction (MAIAC) aerosol optical depth (AOD) fields within the Imperial Valley (**dotted line**) for the WSW (**left**) and SE (**right**) sets. Fields constructed by averaging AOD fields over the cases comprising each respective set (n = 31 for WSW, n = 47 for SE, see Table 2).

Consistency of these spatial patterns with likely areas of windblown dust emissions can be assessed by comparing with sediment supply fields (Figure 7). Within the valley, there is relatively high sediment supply in the northwest valley spanning the Brawley/Westmorland area up to and circling around the southern shore of the Salton Sea to the Niland area. High sediment supply also exists in the desert areas bounding the valley. There is broad visual consistency between the WSW AOD (left panel, Figure 6) and soil sediment fields. Within the valley (dashed lines in the figure), the correlation coefficient of spatially paired points for the two fields is r = 0.30. By comparison, the correlation of spatially paired sediment supply and AOD field for the SE set (right panel, Figure 6) is lower, r = 0.10. This suggests a connection between the higher AOD across the northwest valley in the WSW set and locally generated windblown dust from the high sediment supply areas in the northwestern. valley. Section 3.3 further discusses sources of windblown dust suggested by the analysis.

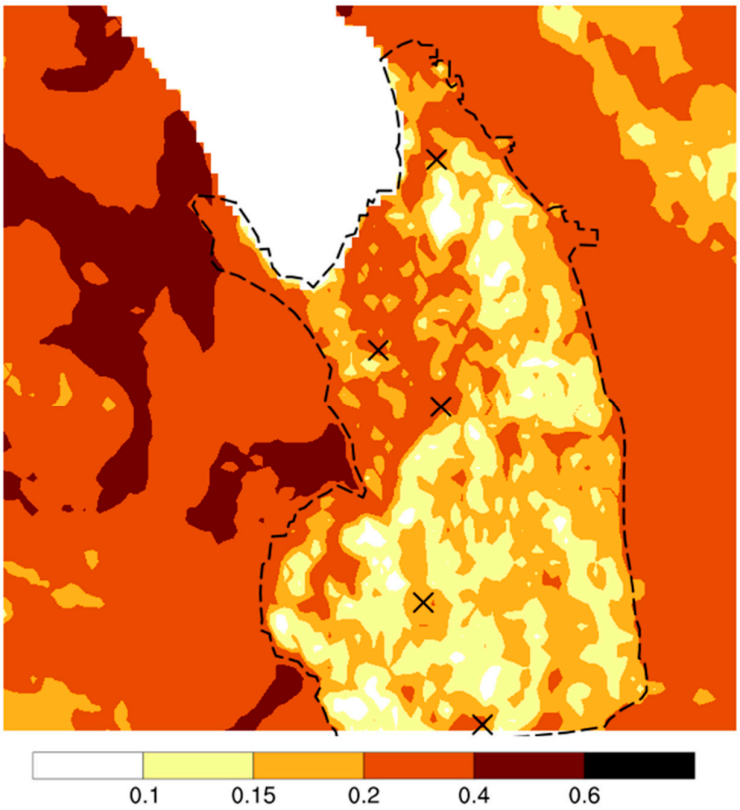

Figure 7. Sediment supply fields over the Imperial Valley and surrounding area from the 500 m global dataset developed by Parajuli and Zender [24]. Field regridded to 1 km to be consistent with the MAIAC AOD fields. The dashed line is as Figure 6, and the "x" symbols indicate locations of routine PM monitors (see Figure 1).

Correspondence of AOD fields with PM measurements for WSW events is assessed separately for 2016 and 2017, the years when IVAN sites were operating. Figure 8 shows the average AOD field overlaid with available ground PM2.5 and PM10 measurements for the 2016 portion of the WSW set. The Brawley-Niland average PM10 concentrations for the 2016 subset and full 2014 to 2017 set are similar (≈130 μg/m^3, see Table 2), and the AOD fields of the two appear broadly similar (comparing the left panel of Figure 6 with Figure 8). The 2016 subset, therefore, appears to be representative of the full WSW set. The AOD and ground PM patterns in Figure 8 are broadly consistent, both exhibiting generally high AOD/PM across the northwestern valley and a distinct high-to-low AOD/PM transition from Brawley/Westmorland southward through the El Centro/Calexico area. The larger relative spatial difference of PM10 (~100 μg/m^3) as compared with PM2.5 (~10 μg/m^3) transitioning north-to-south from the Brawley/Westmorland/Niland to El Centro/Calexico areas is consistent with coarse PM and windblown dust dominating the pattern, as opposed to fine PM sources such as vehicle exhaust, which would cause equal variations in both PM2.5 and PM10. The IVAN measurements provide significant benefit in assessing the correspondence of AOD and PM patterns, particularly helping to confirm the relatively low PM across the southern valley since there are several IVAN sites located away from the two available routine monitors (El Centro and Calexico).

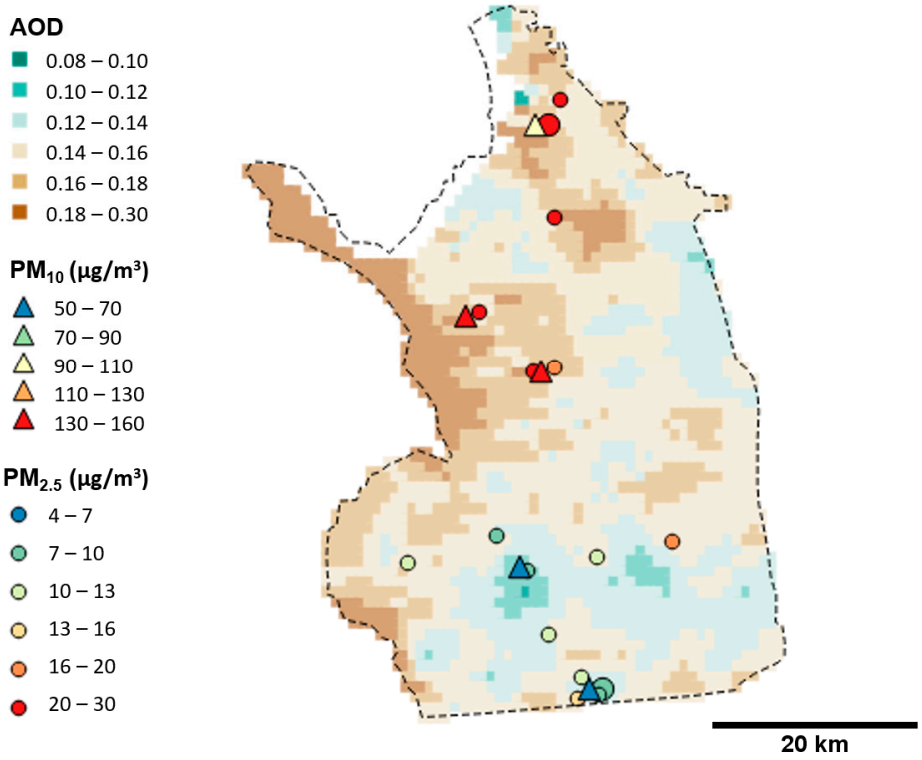

Figure 8. Average MAIAC AOD fields for the WSW set during 2016 (n = 11, see Table 2) overlaid with ground PM concentrations from routine PM10 sites (**large triangles**), routine PM2.5 sites (**large cir**cles), and IVAN PM2.5 sites (**small circles**). Plotted PM10 and PM2.5 concentrations are averages of available measurements over the period at hour encompassing Aqua satellite overpass time.

Figure 9 shows the average AOD field overlaid with available ground PM2.5 and PM10 measurements for the WSW set for 2017. The Brawley-Niland average PM10 concentration for the 2017 WSW events (85 µg/m^3) is lower than the overall value for 2014 to 2017 (130 µg/m^3), and AOD levels across the valley in 2017 are correspondingly lower. Concerning spatial features, since more IVAN monitors were measuring in 2017, more aspects can be assessed. First, it is seen that the broad northwestern area of high AOD/PM in the 2014 to 2017 and 2016 images is fainter than that in 2017. Instead, the 2017 AOD field is dominated more by the localized relatively high AOD areas common to both the WSW and SE sets mentioned earlier. However, while there is broad AOD/PM correspondence in terms of generally higher values in the north as compared with south, no clear correspondence at site level is evident to corroborate these localized features as consistent with ground-level PM. For example, the local AOD hotspot south of Niland, which shows up in all images (2014 to 2017, 2016, and 2017) does not appear to be strongly matched to correspondingly high PM in the available ground measurements in this area. The relatively high AOD in these patchy areas, therefore, may not be indicative of windblown dust hotspots.

Scatterplots of the AOD-PM data paired by day and location for the WSW and SE sets are shown in Figure 10. For the WSW data, correlations are overall very small against IVAN PM2.5 (upper left), while against routine PM10 (lower left) correlations are higher ($r^2 \approx 0.2$), consistent with coarse PM dominating. For the SE data, correlations against both IVAN PM2.5 and routine PM10 (upper and lower right) are weakly positive ($r^2 \approx 0.1$). In general, these low correlations are consistent with what has been found over the western U.S. and California in previous multi-year, regional analyses [29,30]. To explore further, scatterplots of paired AOD-IVAN PM2.5 data averaged by site, to highlight temporal variability, and by day (event), to highlight spatial variability, are presented in Figure 11.

The WSW data is further presented separately for 2016 and 2017. The high spatial correlation in the 2016 WSW data (upper right, Figure 11) is a signature of the consistent spatial AOD and PM variations across the valley this year, as discussed above. By comparison, temporal correlations in the 2016 WSW data (upper left) are low. In the 2017 WSW data (middle panels), both temporal and spatial correlations are low. The 2016 versus 2017 WSW scatterplots, therefore, indicate that although AOD-PM correlations are low overall (Figure 10), MAIAC appears to be able to capture localized average spatial features of windblown PM if levels are high enough. In the SE data (lower panels), the low yet positive correlations in the overall data appear due to AOD capturing broad day-to-day temporal variations, since temporal correlations are around 0.3 and spatial correlations are near zero.

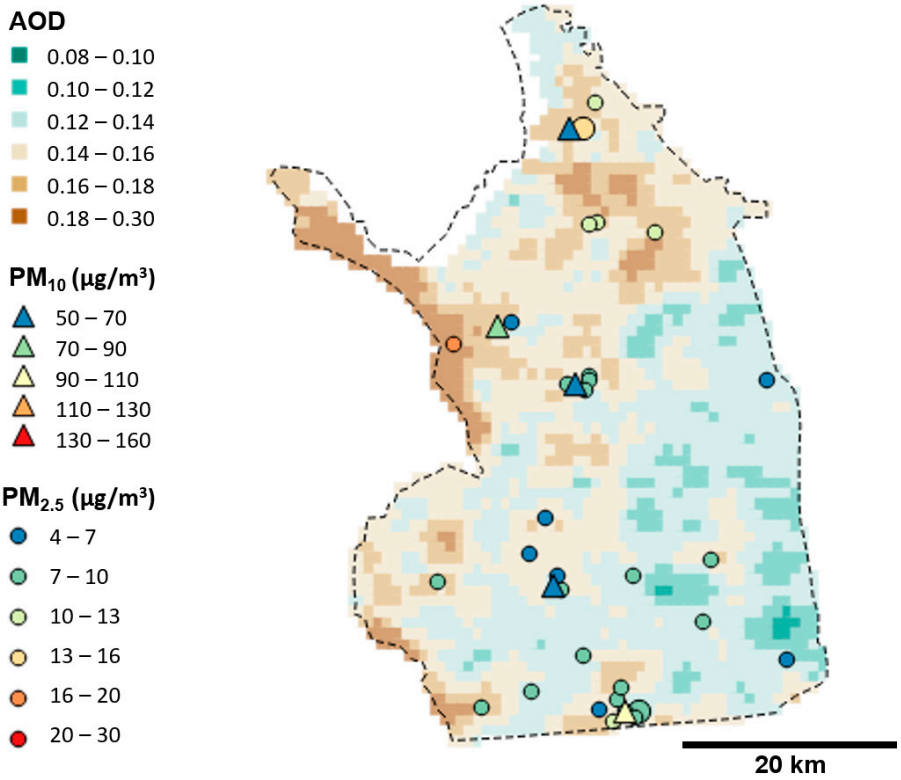

Figure 9. As in Figure 8, but for the WSW set during 2017 (n = 7 days, see Table 2).

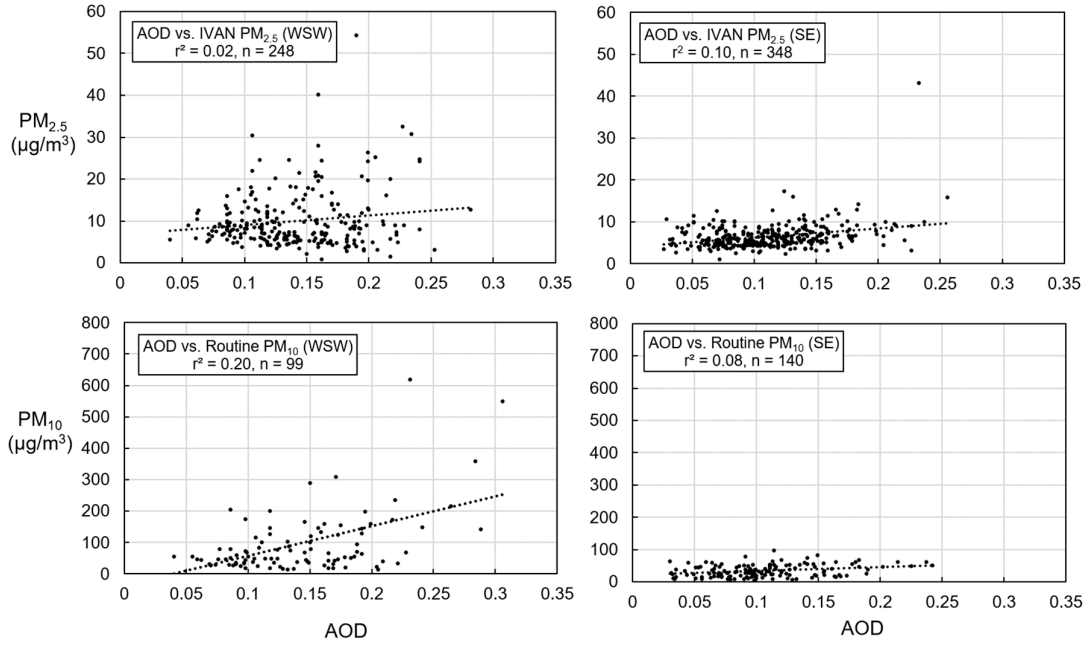

Figure 10. Scatterplots and regression statistics of paired MAIAC AOD and measured PM concentrations at overpass hour; (**top left**) AOD versus IVAN PM2.5 for the WSW set, (**top right**) AOD versus IVAN PM2.5 for the SE set, (**bottom left**) AOD versus routine PM10 for the WSW set, and (**bottom right**) AOD versus routine PM10 for the SE set.

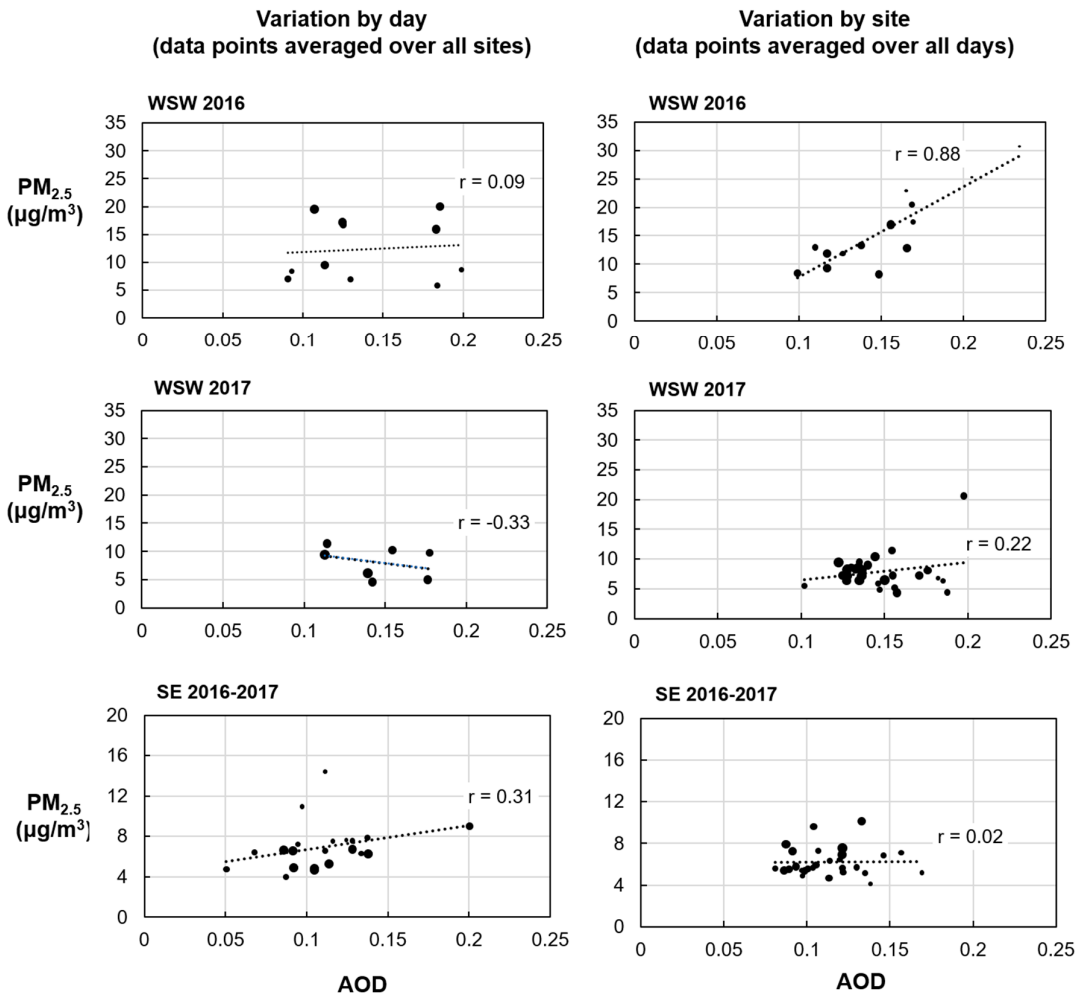

Figure 11. Scatterplots of paired AOD vs. IVAN PM2.5 site and day averaged. Left panels are site averaged to highlight temporal variability across the days comprising sets. Right panels are day averaged to highlight spatial variability across sites comprising sets; (**top**) 2016 WSW, (**middle**) 2017 WSW, and (**bottom**) SE 2016 to 2017. Symbols sized according to the number of paired AOD-PM samples per data point: 7 to 11 sites and 1 to 11 days (WSW 2016); 16 to 26 sites and 2 to 7 days (WSW 2017); 5 to 26 sites and 1 to 22 days (SE 2016 to 2017).

The main points of the detailed analysis are summarized in Figure 12, which shows the transition of the WSW data with successively higher PM10 levels across the events organized as running seven-case averages sorted lowest to highest according to the Brawley-Niland average PM10 concentration of each seven-case average. Seven cases were chosen for the running averages to be a reasonably high number, and consistent with the number of cases comprising the 2017 WSW set. Generally, increasing wind speed and AOD with increasing PM10 across the sorted set is seen (left panel). Viewing AOD patterns across the valley of four selected seven-case averages of successively higher PM10 (right panel), the corroborated area of high AOD spanning the northwest valley first becomes visually clear at PM10 ≈ 100 μg/m^3, and increasingly so, covering the entire northern valley, as PM10 increases to 200 μg/m^3. Below 100 μg/m^3, this feature is not clearly evident, and instead images appear more similar to 2017 (Figure 9) when localized relatively high AOD areas not strongly corroborated by ground PM are predominant. MAIAC, therefore, appears to be able to distinguish surface PM spatial features of windblown dust in the analyzed data during relatively strong WSW events, with PM10 ≈ 100 μg/m^3 appearing to be a rough cutoff when features corroborated by ground monitors become distinguishable. Again, the main feature identified is the broad area of high AOD/PM across the

northwestern valley extending from Brawley-Westmorland towards the southern shore of the Salton Sea and eastward to Niland.

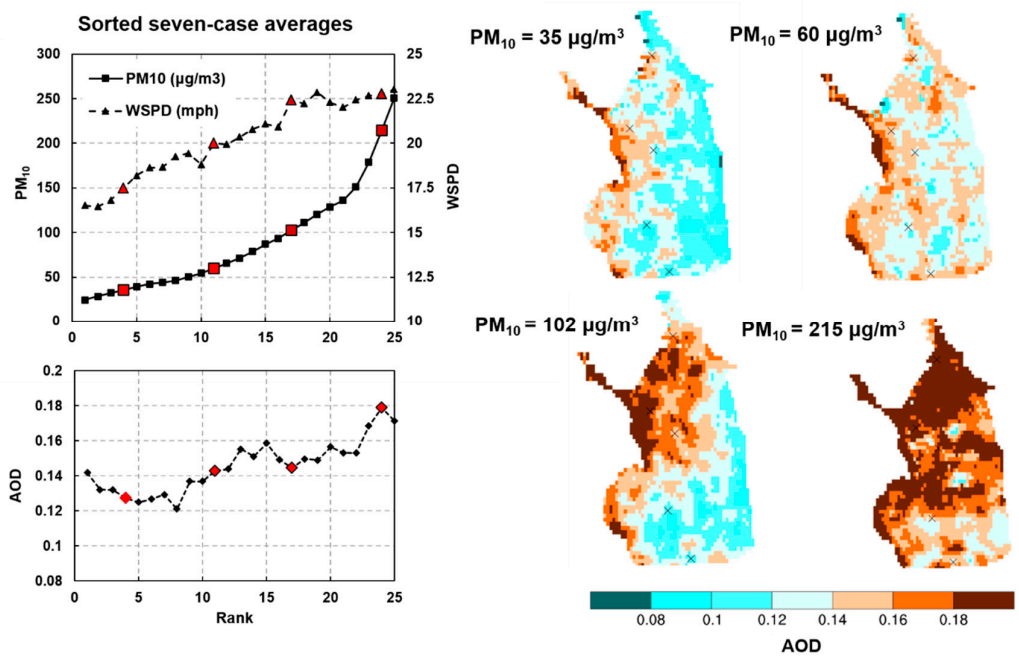

Figure 12. Left: Seven-case running average Brawley-Niland PM10 concentrations for events comprising the WSW set, sorted lowest to highest(solid-squares, **upper left**), and corresponding seven-case running averages for average wind speed at KIPL (dashed-triangles, **upper left**) and valley-averaged AOD (dashed-diamonds, **lower left**). **Right**: spatial plots of seven-case running average AOD fields for four representative points on left-hand plot of successively higher PM10 indicated by red, larger symbols on the left panel. The "x" symbols on right panel are the locations of routine PM10 sites.

3.3. Discussion: Source Areas and Dust Emissions

On the basis of the data analysis, a broad area of the northwestern Imperial Valley spanning the Brawley/Westmorland, southern Salton Sea shore, and Niland area appears especially prone to high PM during windblown dust during strong springtime WSW wind events. The local nature of this feature suggests local sources. The sediment supply field (Figure 7) indicates relatively high values in these same areas as well as over the desert bluff and dune areas immediately to the west (upwind during WSW winds). Erosive loose desert soils, combined with localized increased wind speeds through topographic gaps of this desert complex, are also mentioned by the local air pollution agency [19] as factors increasing dust transport into the valley during westerly windblown dust events. The data analysis presented here adds to this body of evidence pointing to the surfaces of the northwestern valley, the southern Salton Sea shore, and upwind desert areas, in some combination, as dominant local sources affecting the northern Imperial Valley during WSW events. The future impacts on windblown dust from source areas around the Salton Sea could become increasingly important as the sea continues to shrink [17].

More challenging is the determination of the relative contribution of these source areas along with that of the regional background to PM concentrations during WSW events. Ahangar et al. [31] applied dispersion modeling to infer average PM2.5 emissions from broad source areas affecting monthly and annual-averaged IVAN PM2.5 concentrations for year 2017. A similar effort using dispersion models to infer the relative strength of source areas of windblown dust affecting the northwest valley during WSW events could be possible using ambient PM measurements from a specialized field campaign with optimally located monitor sites. While MAIAC AOD was useful in a

time-averaged sense to isolate general areas of high PM and to suggest possible source areas, the low overall correlations in the AOD–PM regressions of paired data suggest difficulty in using AOD quantitatively to augment ground monitoring in such a model inversion exercise, although application of more advanced statistical methods to relate AOD to PM than the simple single-variate regression applied here could prove to be more useful, e.g., [30,32]. Another approach to determine source contributions is the use of detailed composition measurements from candidate source areas (valley versus upwind desert soils, agricultural crop burning areas, and road dust from vehicles) as inputs to receptor models [33].

4. Summary and Conclusions

We examined windblown dust within the Imperial Valley (CA) during events that occurred in spring due to strong west-southwesterly (WSW) winds, which are the most common type affecting the valley. A basic analysis using only routine government meteorological and ambient PM10 and PM2.5 site measurements was first carried out to present a basic understanding. From this analysis, routine site ambient daily-averaged PM10 and PM2.5 concentrations are clearly higher at northern (Westmorland, Brawley, and Niland) as compared with the southern (El Centro and Calexico) valley sites, with PM10 concentrations at the northern sites routinely greater than 100 μg/m^3 and reaching as high as around 400 μg/m^3 for the days analyzed. The daily-averaged PM2.5 concentrations at the northern valley Brawley site were routinely greater than 20 μg/m^3 with the highest value reaching around 60 μg/m^3.

A detailed analysis aimed at better defining the typical spatial PM patterns across the valley for WSW windblown dust conditions was then carried out by augmenting routine observations with the following high-resolution datasets: the IVAN low-cost PM2.5 network of ~40 sites across the valley, the 1 km resolution MAIAC aerosol optical depth (AOD) derived from top-of-atmosphere MODIS radiance retrievals, and 500 m sediment supply fields derived from HydroBASINS upstream catchment and MODIS blue-band surface reflectance. This analysis examined 31 WSW events between 2014 and 2017 with sufficiently high AOD pixel retrieval across the valley for analysis. The clearest finding, based on mutual corroboration of MAIAC AOD, IVAN and routine-site PM measurements, and sediment supply fields, was the identification of a high AOD/PM area during strong WSW events spanning the northwestern valley around Brawley/Westmorland, extending north to the shore of the Salton Sea and Niland area. Lower PM levels were found south of this area, covering El Centro and Calexico. The high AOD/PM area in the northern valley shows up clearly once the average PM10 levels in the northern valley exceed around 100 μg/m^3. This high AOD/PM area corresponds to high sediment supply in this area and immediately upwind within the desert bluff/dune complex west of the valley, suggesting that local dust sources are responsible.

While raw correlations between AOD and PM are low in the data analyzed, temporally averaged correlations (across events to highlight spatial variation in the data) are high for 2016 WSW events, when average PM10 levels were sufficiently high to capture the strong, corroborated AOD/PM feature in the northwestern valley. This is evidence that MAIAC AOD is able to identify high concentration localized spatial areas of PM that typically occur during strong windblown dust events, yet not sensitive enough to identify variations at lower levels or for individual events to be reliably used in these situations..

Concerning uncertainties, the number of episodes investigated in the detailed analysis (31 WSW events) is relatively low, a consequence of our choice to utilize AOD scenes with a high spatial coverage of high quality-flagged pixels. As a result, the number of paired AOD-PM samples are around a few hundred in this study (see Table 2), much less than the 1000 to 10,000 samplesmore common in regional and longer time-period analyses [29,30,34]. The relatively low AOD values, generally below 0.2, also introduce a substantial percentage of noise in data comparison based on the MODIS AOD uncertainty of ±(0.05 + 0.15AOD) [35]. Nonetheless, and especially since clear findings were obtained for the highest PM concentration events analyzed (when AOD values were also higher), we feel the limited data analyzed proved sufficient to draw reasonably clear and useful conclusions.

The results of this study broadly illustrate how MAIAC and a sufficiently dense network of ground observations can be used together to mutually confirm and define spatial patterns associated with strong PM events in local areas. This is encouraging for future efforts by communities and air quality stakeholders to utilize AOD together with low-cost and routine ground PM monitors for local scale air quality analysis, historically limited due to sole availability of sparsely spaced routine monitors. The use of the IVAN community-collected PM data in this study also shows how a citizen science effort to collect more spatially refined air quality information can help pinpoint episodic pollution patterns and possible sources important for reducing PM exposure and adverse health effects.

Author Contributions: Conceptualization, F.F., P.E., J.W., Y.L., and A.V.; methodology, F.F.; formal analysis, F.F.; resources, P.E. M.S.-H., R.C., and M.A.-H.; writing—original draft, F.F, P.E., J.W., and D.T.; writing—review and editing, all authors; visualization, F.F. and A.R.; funding acquisition, P.K. All authors have read and agreed to the published version of the manuscript.

Funding: These authors received the following funding for this study from the NASA Health and Air Quality Applied Sciences Team : F.F, A.V., and M.A.-H. (NASA grant NNX16AQ91G), Y.L. (NNX16AQ28G), D.T. (NNX16AQ19G), and P.K. (NNX16AQ20G).

Acknowledgments: The authors acknowledge the Imperial Valley Air Network (IVAN) team of researchers and stakeholders at Comite Civico Del Valle, Inc., Tracking California, and the University of Washington for providing and assisting us in utilizing the IVAN air monitoring data for this study. See https://ivan-imperial.org/ for more details about the IVAN monitoring program. We also acknowledge Alexei Lyapustin for helpful discussions about MAIAC.

Conflicts of Interest: The authors declare no conflict of interest. The funders had no role in the design of the study; in the collection, analyses, or interpretation of data; in the writing of the manuscript, or in the decision to publish the results.

Appendix A

For the detailed analysis, we analyzed 31 WSW events from 2014 to 2017. An event is defined as a day occurring from March through June when the KIPL wind speed averaged over 1200 to 1400 LST was above 10 mph, and the wind direction scalar averaged over these hours was between 230 and 280 degrees. This procedure produced 82 daily cases. From this larger set, we selected 31 when AOD coverage was deemed complete enough across the valley for further analysis. Plots of 1200 to 1400 LST averaged PM10 concentrations at the Brawley and Niland BAMS routine sites versus wind speed averaged over this time period at the KIPL for the larger 82 versus the chosen 31 days are shown in Figure A1. The PM10 concentrations and their relationship to wind speed for the 31 days reasonably matches those from the larger set, and hence the analyzed set of 31 cases appears representative for further analysis.

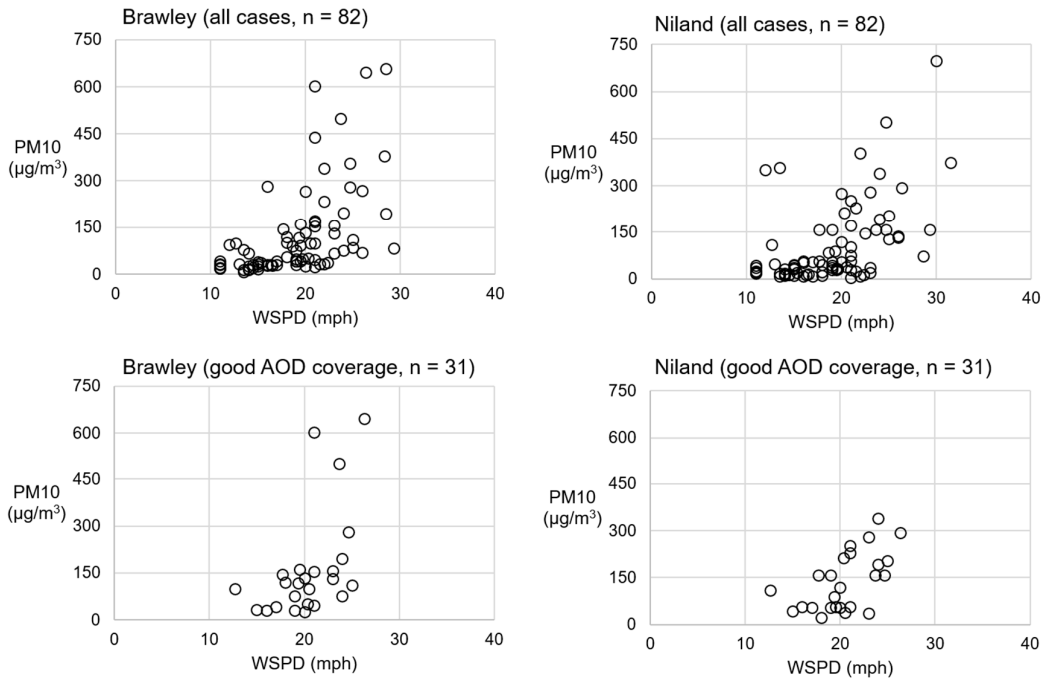

Figure A1. PM10 concentrations averaged over 1200 to 1400 LST at Brawley (**left panels**) and Niland-English Road (**right panels**) versus wind speed at KIPL averaged over 1200 to 1400 LST for days screened for wind speeds greater than 10 miles per hour and wind direction between 230 and 280 degrees. The top panels are all screened days and the bottom panels are subset for which AOD spatial coverage was deemed sufficient for final analysis.

References

1. Chronology of State PM10 Designations. Available online: https://www.arb.ca.gov/desig/changes/pm10.pdf (accessed on 13 November 2019).
2. Annual Report on the California Air Resources Board's Fine Particulate Monitoring Program. Available online: https://www.arb.ca.gov/research/apr/reports/pm25-monitoring-2018.pdf (accessed on 13 November 2019).
3. Tracking California, Public Health Institute. Asthma Related Emergency Department & Hospitalization data: Asthma. Available online: www.trackingcalifornia.org/asthma/query (accessed on 13 November 2019).
4. Pope, C.A.; Dockery, D.W. Health effects of fine particulate air pollution: Lines that connect. *J. Air Waste Manag. Assoc*. **2006**, *56*, 709–742. doi:10.1080/10473289.2006.10464485.
5. Lee, S.H.; Wong, H.; Lau, Y. Association between air pollution and asthma admission among children in Hong Kong. *Clin. Exp. Allergy* **2006**, *36*, 1138–1146.
6. Adar, S.P.; Filigrana, N.; Clements, J.P. Ambient Coarse Particulate Matter and Human Health: A Systematic Review and Meta-Analysis. *Cur. Environ. Health Rep.* **2014**, *1*, 258–274.
7. Crooks, L.J.; Cascio, E.W.; Percy, S.M.; Reyes, J.; Neas, M.L.; Hilborn, D.E. The association between dust storms and daily non-accidental mortality in the United States, 1993–2005. *Environ. Health Perspect.* **2016**, *124*, 1735.
8. Rice, M.B.; Mittleman, M.A. Dust storms, heart attacks, and protecting those at risk. *Eur. Heart J.* **2017**, *38*, 3209–3210. doi:10.1093/eurheartj/ehx550.
9. CDC. Increase in reported coccidioidomycosis--United States, 1998–2011. *Morb. Mortal. Wkly. Rep*. **2013**, *62*, 217.
10. Tong, D.Q.; Wang, J.X.; Gill, T.E.; Lei, H.; Wang, B. Intensified dust storm activity and Valley fever infection in the southwestern United States. *Geophys. Res. Lett.* **2017**, *44*, 4304–4312.

11. Chow, J.C.; Watson, J.G.; Green, M.C.; Lowenthal, D.H.; Bates, B.; Oslund, W.; Torres, G. Cross-border transport and spatial variability of suspended particles in Mexicali and California's Imperial Valley. *Atmos. Environ.* **2000**, *34*, 1833–1843.
12. Wagner, J.; Casuccio, G. Spectral imaging and passive sampling to investigate particle sources in urban desert regions. *Environ. Sci. Process. Impacts* **2014**, *16*, 1745–1753. doi:10.1039/C4EM00123K.
13. King, J.; Etyemezian, V.; Sweeney, M.; Buck, B.J.; Nikolich, G. Dust emission variability at the Salton Sea, California, USA. *Aeolian Res.* **2011**, *3*, 67–79. doi:10.1016/j.aeolia.2011.03.005.
14. Buck, B.J.; King, J.; Etyemezian, V. Effects of Salt Mineralogy on Dust Emissions, Salton Sea, California. *Soil Sci. Soc. Am. J.* **2011**, *71*, 1971–1985. doi:10.2136/sssaj2011.0049.
15. Cohen, M.J. Hazard's Toll: The Cost of Inaction at the Salton Sea. *Pac. Inst.* **September 014**. Available online: https://pacinst.org/publication/hazards-toll/ (accessed on 15 March 2019).
16. Frie, A.L.; Dingle, J.H.; Ying, S.C.; Bahreini, R. The Effect of a Receding Saline Lake (The Salton Sea) on Airborne Particulate Matter Composition. *Environ. Sci. Technol.* **2017**, *51*, 8283–8292. doi:10.1021/acs.est.7b01773.
17. Parajuli, S.P.; Zender, C.S. Projected changes in dust emissions and regional air quality due to the shrinking Salton Sea. *Aeolian Res.* **2018**, *33*, 82–92. doi: 10.1016/j.aeolia.2018.05.004.
18. Johnston, J.; Razafy, M.; Lugo, H.; Olmedo, L.; Farzan, S.F. The Disappearing Salton Sea: A Critical Reflection on the Emerging Environmental Threat of Disappearing Saline Lakes and Potential Impacts on Children's Health. *Sci. Total. Environ*. **2019**, *663*. doi:10.1016/j.scitotenv.2019.01.365.
19. ICAPCD. High Wind Exceptional Event Fugitive Dust Mitigation Plan for Imperial County. 2019. Available online: https://www.co.imperial.ca.us/AirPollution/otherpdfs/MitigationPlan.pdf (accessed on 15 October 2019).
20. English, P.B.; Olmedo, L.; Bejarano, E.; Lugo, H.; Murillo, E.; Seto, E.; Wong, M.; King, G.; Wilkie, A.; Meltzer, D.; et al. The Imperial County Community Air Monitoring Network: A Model for Community-based Environmental Monitoring for Public Health Action. *Environ. Health Per.* **2017**, *125*, 7. doi:10.1289/EHP1772.
21. Carvlin, G.N.; Lugo, H.; Olmedo, L.; Bejarano, E.; Wilkie, A.; Meltzer, D.; Wong, M.; King, G.; Northcross, A.; Jerrett, M.; et al. Development and field validation of a community-engaged particulate matter air quality monitoring network in Imperial, California, USA. *J. Air Waste Manag. Assoc.* **2017**, *67*, 1342–1352. doi:10.1080/10962247.2017.1369471.
22. Wong, M.; Bejarano, E.; Carvlin, G.; Fellows, K.; King, G.; Lugo, H.; Jerrett, M.; Meltzer, D.; Northcross, A.; Olmedo, L.; et al. Combining Community Engagement and Scientific Approaches in Next-Generation Monitor Siting: The Case of the Imperial County Community Air Network. *Int. J. Environ. Res. Pub. Health* **2018**, *15*. doi:10.3390/ijerph15030523.
23. Lyapustin, A.; Wang, Y.; Korkin, S.; Huang, D. MODIS Collection 6 MAIAC algorithm. *Atmos. Meas. Tech*. **2018**, *11*, 5741–5765. doi:0.5194/amt-11-5741-2018.
24. Parajuli, S.P.; Zender, C.S. Connecting geomorphology to dust emission through high-resolution mapping of global land cover and sediment supply. *Aeolian Res.* **2017**, *27*, 47–65. doi:10.1016/j.aeolia.2017.06.002.
25. California Air Resources Board, Air Quality and Meteorological Information System. Available online: https://www.arb.ca.gov/aqmis2/aqmis2.php (accessed on 13 November 2019).
26. Mesowest. Available online: https://mesowest.utah.edu/ (accessed on 13 November 2019).
27. LAADS DAAC, Multi-Angle Implementation of Atmospheric Correction (MAIAC). Available online: https://ladsweb.modaps.eosdis.nasa.gov/missions-and-measurements/science-domain/maiac (accessed on 13 November 2019).
28. Mesinger, F.; DiMego, G.; Kalnay, E.; Mitchell, K.; Shafran, P.C.; Ebisuzaki, W.; Jović, D.; Woollen, J.; Rogers, E.; Berbery, E.H.; et al. North American Regional Reanalysis. *Bull. Amer. Meteor. Soc.* **2006**, *87*, 343–360. doi:10.1175/BAMS-87-3-343.
29. Zhang, H.; Hoff, R.M.; Engle-Cox, J.A. The Relation between Moderate Resolution Imaging Spectroradiometer (MODIS) Aerosol Optical Depth and PM2.5 over the United States: A Geographical Comparison by U.S. Environmental Protection Agency Regions. *J. Air Waste Manag. Assoc.* **2009**, *59*, 1358–1369. doi:10.3155/1047-3289.59.11.1358.
30. Lee, H.J.; Chatfield, R.C.; Strawa, A.W. Enhancing the Applicability of Satellite Remote Sensing for PM2.5 Estimation Using MODIS Deep Blue AOD and Land Use Regression in California, United States. *Environ. Sci. Tech.* **2016**, *50*, 6546–6555. doi:10.1021/acs.est.6b01438.

31. Ahangar, F.E.; Freedman, F.R.; Venkatram, A. Using Low-Cost Air Quality Sensor Networks to Improve the Spatial and Temporal Resolution of Concentration Maps. *Int. J. Environ. Res. Pub. Health* **2019**, *16*. doi:10.3390/ijerph16071252.
32. Kloog, I.; Sorek-Hamer, M.; Lyapustin, A.; Coull, B.; Wang, Y.; Just, A.C.; Schwartz, J.; Broday, D.M. Estimating daily PM2.5 and PM10 across the complex geo-climate region of Israel using MAIAC satellite based AOD data. *Atmos. Environ*. **2015**. doi:10.1016/j.atmosenv.2015.10.004.
33. Watson, J.G.; Zhu, T.; Chow, JC.; Engelbrecht, J.; Fujita, E.M.; Wilson, W.E. Receptor modeling application framework for particle source apportionment. *Chemosphere* **2002**, *49*, 1093–1136. doi:10.1016/S0045-6535(02)00243-6.
34. Gupta, P.; Doraiswamy, P.; Levy, R.; Pikelnaya, O.; Maibach, J.; Feenstra, B.; Polidori, A.; Kiros, F.; Mills, K.C. Impact of California Fires on Local and Regional Air Quality: The Role of a Low-Cost Sensor Network and Satellite Observations. *Geohealth* **2018**, *2*, 172–181. doi:10.1029/2018GH000136.
35. Levy, R.C.; Mattoo, S.; Munchak, L.A.; Remer, L.A.; Sayer, A.M.; Patadia, F.; Hsu, N.C. The Collection 6 MODIS aerosol products over land and ocean. *Atmos. Meas. Tech*. **2013**, *6*, 2989–3034. doi:10.5194/amt-6-2989-2013.